# 3-D Ray Launching MIMO Channel Geometric Estimation

Fidel Alejandro Rodríguez-Corbo ⓘ, *Student Member, IEEE*, Leyre Azpilicueta ⓘ, *Senior Member, IEEE*,
Mikel Celaya-Echarri ⓘ, *Member, IEEE*, Raed Shubair ⓘ, *Senior Member, IEEE*,
and Francisco Falcone ⓘ, *Senior Member, IEEE*

*Abstract*—The complete multiple-input–multiple-output (MIMO) channel simulation in deterministic techniques can be a computationally intensive task, due to the inherent scenario's complexity and number of antennas. The spatial coherence among MIMO elements is a reasonable assumption to approximate the channel from a single point simulation. In this letter, a novel method to incorporate a geometrical approximation of the MIMO channel into a three-dimensional ray launching (3D-RL) algorithm is presented. The method is antenna type independent and the orientation of the array is embedded in the antenna representation. Relevant information of the MIMO channel characteristics like the root mean square (rms) delay spread, the maximum delay spread, phase and channel capacity are obtained and compared with the full 3D-RL simulation of the entire MIMO array, achieving 93.4% reduction in computational time.

*Index Terms*—Channel response, Hesse normal form, multiple-input–multiple-output (MIMO), ray launching.

## I. INTRODUCTION

**M**ULTIPLE antenna systems allow the use of spatial/temporal diversity, which brings many advantages in the wireless link, such as increased network capacity, diversity gain, and reliability. There are multiple techniques for modeling the communication channel in multiple-input–multiple-output (MIMO) systems, with the main joint drawback of high computational capacities. An increase in the ability to generate more precise and complex three-dimensional (3-D) environments with new path estimation techniques, has led to deterministic techniques such as ray tracing/ray launching (RT/RL) methods to gain popularity in recent years. These techniques are based on high-frequency approximations of electromagnetic wave propagation using geometric optics and the uniform theory of

diffraction (UTD). RT/RL methods are site-specific and require detailed information of the considered scenario, as well as all the electromagnetic material properties at the system operating frequency. The simulation computational cost in these methods can escalate very quickly if a MIMO system is implemented in the transducers, as simulations must be performed for each MIMO antenna element, thus increasing an already complex modeling algorithm [1].

One approach to solve this problem of multiantenna simulations is the use of virtual point approximations [2]. This method takes advantage of the reasonable spatial coherence that exists between the array elements since the spacing between the elements is relatively small and typically on the order of half to a few wavelengths. This is especially true for high frequency communications such as mmWave frequencies. Thus, it can be assumed that multipath components and their consequent power contributions are identical in all the elements, only changing the phase of each contribution referenced to the spatial displacement with respect to a simulated virtual single point. The advantages of this method are evident in a RT/RL simulation, as the complex multiantenna simulations can be reduced to a single-input–single-output (SISO) simulation between virtual points, and the obtained information can be extrapolated to the rest of the array elements. This method is independent of the array size so multiple types of arrays can be used with just one simulation.

### A. Related Works

In [2], the comparison of a virtual point approximation method against a full point-to-point simulation called brute force is performed at 1.92 GHz frequency, showing that the virtual point approximation method for uniform arrays produces a negligible error in most conditions and contributes to a considerable reduction in simulation time. In [3], the capacity of the MIMO communication channel is evaluated using the RT technique at 2.5 GHz center frequency. The virtual point approximation method is used and numerical estimations for a uniform linear array (ULA) and a circular antenna array are presented. Moreover, other works present the use of geometrical approximations to estimate the phase changes for specific MIMO antenna types, such as uniform arrays [4], [5], or uniform concentric circular array [6]. Systems at mmWave and THz frequency bands can benefit from this virtual point approximation method, as the dimensions of the arrays at these frequencies are more conservative with the assumption of spatial coherence [7]. In reference [8], an analysis of the system capacity impact of this virtual point approximation method is presented, concluding that the use of massive MIMO
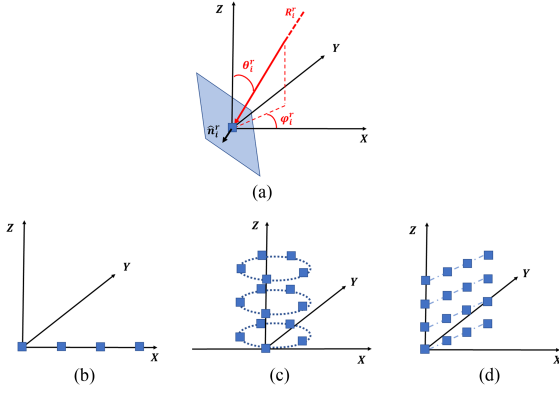
Fig. 1. (a) Self-contained coordinate system implemented at an antenna array element in the 3D-RL algorithm. (b)–(d) Different antenna array configurations.

systems and large arrays can increase the approximation errors in a virtual point method. Thus, further studies are needed, especially in their use for millimeter band frequency systems.

### B. Our Contributions

The aim of this study is encouraged by the need to provide and validate an accurate general antenna type method, to estimate a MIMO channel response using the virtual point approximation at mmWave frequency bands. In this regard, for the author's knowledge, there are not many studies at mmWave frequencies under non-stationarity conditions, and most of them use a specific type of antenna configuration to accommodate the setup calculation. Therefore, with the aim to fill this gap, this letter presents a novel methodology implemented in an in-house three-dimensional ray launching (3D-RL) simulator for the acquisition of the MIMO channel response, considering antenna type independence, with embedded orientation antenna setup, coupled with the nonstationarity simulation of the software as an Addon. Finally, the validation of the proposed methodology is provided, by comparing MIMO channel characteristics with the full 3D-RL simulation of the entire MIMO array.

## II. MIMO CHANNEL METHODOLOGY

As stated before, the main disadvantage of a brute force RT/RL simulation comes from the high computational cost of tracking every ray and consequently propagation phenomena that may be present for every antenna array element. With the assumption of a plane wavefront and exploiting the spatial coherence between array elements, the difference in phase for all antenna elements can be approximated using the ray angle-of-arrival/angle-of-departure, the relative antenna steering orientation, and the array elements relative distances. These calculations can be adjusted for any kind of MIMO array [1], [3], but can hold an inherent complexity when implementing into a 3D-RL algorithm for all antenna configuration, shape, or 3D steering orientation angle of the antenna array. To solve this problem, a Hesse normal form representation of the planar wavefront is used in order to easily estimate the point-plane distance for every array element in a 3D representation. For this purpose, an independent self-contained coordinate system is implemented with the origin set at an antenna element of the array, as it is represented in Fig. 1(a). From this centered element, all information can be extrapolated using the point-to-point simulation result from the 3D-RL algorithm.

Equation (1) represent the Hesse normal form for a plane crossing the origin, the coordinate indexes are contained in $\boldsymbol{p} = [x, y, z]^{\mathrm{T}}$ and $\hat{\boldsymbol{n}}_i^{t\backslash r}$ is the unit normal vector to the planar wavefront for the $i$th path. The top indexes represent the transmitted ($t$) or received ($r$) path.

$$\hat{\boldsymbol{n}}_i^{t\backslash r} \cdot \boldsymbol{p} = 0 \qquad (1)$$

where

$$\hat{\boldsymbol{n}}_i^{t\backslash r} = \begin{bmatrix} -\sin\theta_i^{t\backslash r}\cos\varphi_i^{t\backslash r} \\ -\sin\theta_i^{t\backslash r}\sin\varphi_i^{t\backslash r} \\ -\cos\theta_i^{t\backslash r} \end{bmatrix}. \qquad (2)$$

The normal vector $\hat{\boldsymbol{n}}_i$ is a unitary representation of the arrival/departure ray ($\mathrm{R}_i^{t\backslash r}$) as seen in Fig. 1(a), using the negative vector depiction in order to project the normal vector in the opposite side of the plane. Thus, the signed point-plane distance $\mathrm{D}_{im}^{t\backslash r}$ to a point $\boldsymbol{p}_m = [x_m, y_m, z_m]^{\mathrm{T}}$ can be found as

$$D_{im}^{t\backslash r} = \hat{\boldsymbol{n}}_i^{t\backslash r} \cdot \boldsymbol{p}_m \qquad (3)$$

where $m$ is the antenna element index. Consequently, with all the elements in the antenna array correctly defined within this reference frame, the planar wavefront to point antenna element distance/phase can be easily calculated. Considering this approach, all antenna configurations or shapes can be represented, and steering angles can be set if the self-reference coordinate is aligned to the one of the 3D-RL simulation. Fig. 1(b)–(d) presents different possible example configurations that can be implemented, like ULA (1b), cylindrical (1c), or tilted planar array (1d), among others. Full phase characteristics can be approximated for all antenna elements within the MIMO array. To this end, the narrowband full MIMO channel matrix $\mathbf{H}$ is given by

$$\mathbf{H} = \sum_i a_i \boldsymbol{e_r}(i)\,\boldsymbol{e_t}(i)^{\mathrm{T}} \qquad (4)$$

where

$$a_i = \alpha_i\,\sqrt{n_t n_r}\,exp\left(-j2\pi\gamma_i\right) \qquad (5)$$

$$\boldsymbol{e_r}(i) = \frac{1}{\sqrt{n_r}}\begin{bmatrix} \exp\left(-j2\pi D_{i0}^r\right) \\ \exp\left(-j2\pi D_{i1}^r\right) \\ \vdots \\ exp\left(-j2\pi D_{i(n_r-1)}^r\right) \end{bmatrix} \qquad (6)$$

$$\boldsymbol{e_t}(i) = \frac{1}{\sqrt{n_t}}\begin{bmatrix} \exp\left(-j2\pi D_{i0}^t\right) \\ \exp\left(-j2\pi D_{i1}^t\right) \\ \vdots \\ exp\left(-j2\pi D_{i(n_t-1)}^t\right) \end{bmatrix} \qquad (7)$$

where $n_t$ and $n_r$ are the number of antennas at the transmitter and receiver array respectively, $\alpha_i$ and $\gamma_i$ are the complex gain amplitude and the phase information for the $i$th path, respectively, between the SISO transmit virtual point and receiver virtual point 3D-RL simulation. Also, $\boldsymbol{e_r}(i)$ and $\boldsymbol{e_t}(i)$ are known as the unit spatial signature in the propagation direction of path $i$, for receiver and transmitter, respectively. It can be found that if the coordinate system for the MIMO array representation is normalized to the wavelength $\lambda_c$ of the carrier, the phase shifts in the spatial signatures are captured by the relative distance $D_{im}^{t\backslash r}$, where $m$ is the antenna element index from 1 to $n_{t\backslash r}-1$, and each element is associated to its relative point position $\boldsymbol{p}_m$ from (3). Although the virtual point can be located anywhere in
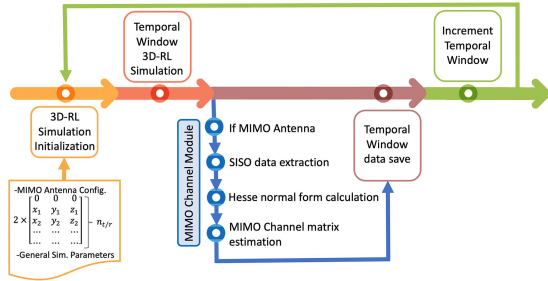
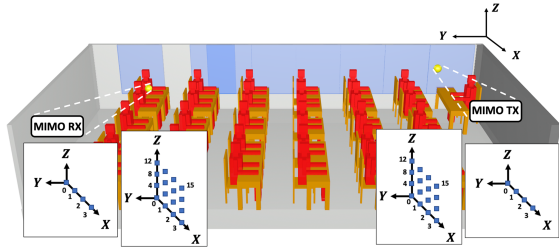Fig. 2.     MIMO channel post-processing flow diagram.



Fig. 3.     3D-RL test scenario.

the 3D MIMO representation, in this letter, we use a centered antenna element from the array. Thus, the point-plane distance for this element is 0, and the first component in the vectors $e_r(i)$ and $e_t(i)$ becomes 1.

## III. 3D-RL IMPLEMENTATION

An in-house 3D-RL MATLAB-based algorithm has been used for the implementation of the proposed method. The algorithm considers all the electromagnetic phenomena in the environment, as well as material properties for all the obstacles at the operating simulation frequency [9], [10]. The method to determine the MIMO channel matrix from SISO simulations is performed as a post-processing stage and it has been integrated as an Addon feature. The 3D-RL algorithm is also designed to assess mobility scenarios uninterruptedly, so the information pertaining to each temporal state of the MIMO array is introduced in each state of the temporal characteristics of the simulation. At this point, the only information needed is the array layout within the temporal window that is going to be simulated. This information is fed to the software through two matrixes, $n_t \times 3$ and $n_r \times 3$, where each row is an antenna index starting from the origin ($[0, 0, 0]$), up to the last antenna element in the array. As the coordinate system is parallel to the one in the 3D-RL software, relative tilted information of the array can be aggregated using a tilted representation in the self-contained coordinate system of the array. Fig. 2 shows a flow chart of the 3D-RL simulation and the added MIMO channel estimation feature.

In order to assess and validate the method, an indoor test scenario has been implemented in the 3D-RL algorithm. The scenario is a typical classroom where two different types of antenna array structures have been considered for validation purposes in both transceivers: a 4-element ULA and a 16-element uniform planar array (UPA). The carrier frequency is 28 GHz, while the transmitter is located near the classroom ceiling and the receiver is located at 1.6 m above the ground, emulating a student sitting at the end of the classroom. Fig. 3 shows the layout of the stage,
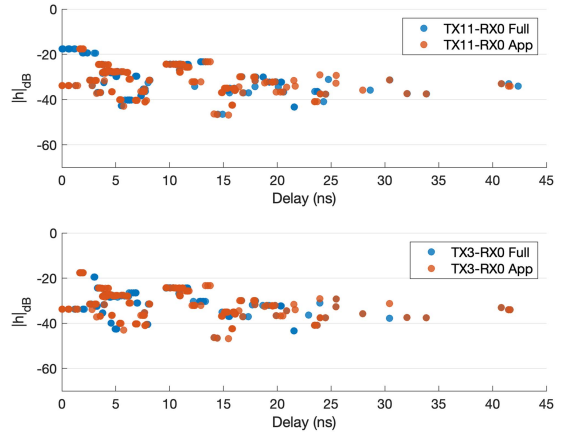




Fig. 4.     Channel impulse response comparison for the approximation method and complete 3D-RL simulation method: between TX11 y RX0 in 16-UPA-MIMO (up); between TX3 and RX0 in 4-ULA-MIMO (down).

as well as the locations of the different considered radiating elements.

The element spacing in the ULA antenna is $(1/2)\lambda_c$. Thus, given a $\lambda_c$ normalization and assigning $\Delta_{t\backslash r} = 1/2$ as the normalized space between elements, it can be found that for an ULA antenna in position like Fig. 1(b), (3) is reduced to

$$D_{im}^{t\backslash r} = m * \Delta_{t\backslash r} * (-\sin\theta_i^{t\backslash r} \cos\varphi_i^{t\backslash r}) \qquad (8)$$

where $1 \le m \le n_{t\backslash r} - 1$ is the antenna element index. This result coincides with the typical ULA geometrical approximation that can be found in the literature [8].

## IV. RESULTS AND DISCUSSIONS

In order to establish evaluative comparisons of the method, the 3D-RL complete MIMO channel simulation is performed for all the array elements in both cases, and it has been compared with the approximation method, where one element per array is needed (SISO simulation). The actual complex channel response is considered for comparison, with the channel response amplitude, phase, and capacity. Fig. 4 shows the channel response amplitude profile between two individual MIMO array elements for both analyzed cases.

The representation of the magnitude is adequately captured by the approximation method, describing it with relative similarity characteristic elements, such as the root mean square delay spread (Rms-DS) and the maximum excess delay. A cross-correlation measure can be calculated by means of the following equation, given a resampling of the signals with a multipath time resolution of $\Delta_\tau = 0.5 \, ns$ bin:

$$\rho\left(h_{t,r}^{app}, h_{t,r}^{full}\right)$$

$$= \frac{\sum_{s=1}^{M}\left(h_{t,r}^{app}(s * \Delta_\tau) * h_{t,r}^{full}(s * \Delta_\tau)\right)}{\max\left\{\sum_{s=1}^{M}\left(h_{t,r}^{app}(s*\Delta_\tau)^2\right), \sum_{s=1}^{M}\left(h_{t,r}^{full}(s*\Delta_\tau)^2\right)\right\}} \qquad (9)$$

where $\rho(h_{t,r}^{app}, h_{t,r}^{full})$ is the correlation coefficient, $h_{t,r}^{app}$ and $h_{t,r}^{full}$ are the channel response profiles of the approximation and the full 3D-RL simulation respectively, $0 \le t \le 3/15$ and $0 \le r \le 3/15$ are the elements indexes (transmitter and receiver respectively), and $M$ is the maximum excess delay between

TABLE I
CHANNEL RESPONSE AMPLITUDE PREDICTIONS PERFORMANCE COMPARISON

| 4-ULA-MIMO | | $\|h_{3,0}\|$ | $\|h_{2,1}\|$ | $\|h_{1,2}\|$ | $\|h_{0,3}\|$ |
|---|---|---|---|---|---|
| Rms-DS | 3D-RL | 5.41 ns | 5.46 ns | 5.33 ns | 5.27 ns |
| | Approx. | 5.61 ns | 5.61 ns | 5.61 ns | 5.61 ns |
| Max. excess delay | 3D-RL | 42.9 ns | 42.1 ns | 42.1 ns | 41.6 ns |
| | Approx. | 41.6 ns | 41.6 ns | 41.6 ns | 41.6 ns |
| $\rho\left(h_{t,r}^{app}, h_{t,r}^{full}\right)$ | | 0.7 | 0.56 | 0.94 | 0.97 |
| 16-UPA-MIMO | | $\|h_{12,2}\|$ | $\|h_{12,4}\|$ | $\|h_{12,10}\|$ | $\|h_{12,14}\|$ |
| Rms-DS | 3D-RL | 3.77ns | 3.50 ns | 4.94 ns | 4.85 ns |
| | Approx. | 3.71 ns | 3.71 ns | 3.71 ns | 3.71 ns |
| Max. excess delay | 3D-RL | 42.1 ns | 41.6 ns | 42.3 ns | 42.7 ns |
| | Approx. | 42.6 ns | 41.6 ns | 41.6 ns | 41.6 ns |
| $\rho\left(h_{t,r}^{app}, h_{t,r}^{full}\right)$ | | 0.81 | 0.62 | 0.13 | 0.24 |



Fig. 5.    Phase RAE in the approximation method: (a) 4-ULA and (b) 16-UPA.



Fig. 6.    MIMO channel capacity (full 3D-RL simulation versus approximation method): (a) 4-ULA and (b) 16-UPA.
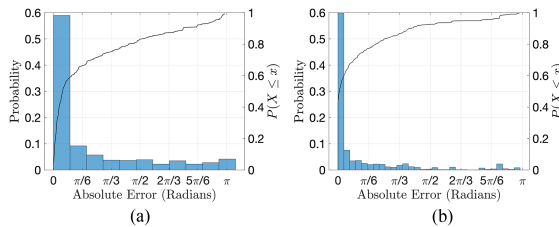
the delay profiles in number of bins. Table I summarizes these characteristics for 4 SISO channel responses.

The displayed error in the magnitude of individual paths is related to the changes in the path attenuation from one element to another, although typically these attenuations change slowly on the scales of distances in an mmWave frequency array. Overall, the mean correlation across all individual channels is 0.78 for the 4-ULA antenna and 0.41 for the 16-UPA. As the virtual simulated point is mutual in both cases, the mean correlation is lower in the 16-UPA case due to the corresponding further distances of the different array elements. On the other hand, the phases of these paths change drastically in distances of fractions of wavelength, being an influential factor in the constructive or destructive association of the different paths. The assumptions of a flat wavefront, and the reuse of the arriving/departing paths in the SISO simulation towards the rest of the elements is the force driving the errors in the estimation. Fig. 5 shows the relative absolute error (RAE) between the phases of the multipaths described by the approximation method and the complete 3D-RL simulation for both antenna array structures.

From the figures, the high volume of phase RAE clusters near the lower measure of error in both cases. Thus, most of the paths are accurately phase estimated or with low error, where the mean obtained error is 38.4 degrees for the 4-ULA antenna and 21.6 degrees for the 16-UPA antenna. Another measure of similarity is the estimation of the cross-correlation using (9), deriving a mean correlation of 0.77 and 0.48, for the 4-ULA and 16-UPA, respectively.

Next, the system capacity has been analyzed and compared for both array structures. The system capacity is determined with channel state information at the receiver (CSIR). Therefore, the data is transmitted independently in each of the transmitting antennas and the transmission power is equally distributed among the elements, applying an effective power of $P/n_t$ on each transmission element. In this configuration the resulting
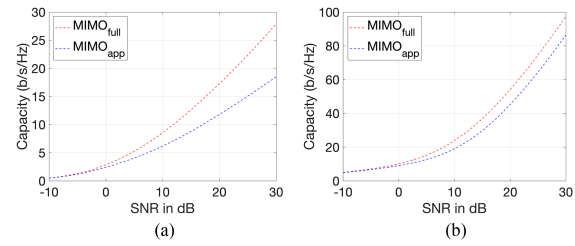
capacity is [11]

$$C = log\left(\mathbf{I}_{n_r} + \frac{SNR}{n_t}\mathbf{H}_n\mathbf{H}_n^*\right) \quad (10)$$

where $\mathbf{H}_n$ is the normalized channel response matrix and is determined as $\|\mathrm{H}\|_F^2 = n_r * n_t$, $\mathbf{I}_{(n_r)}$ is the $n_r$ identity matrix and $SNR$ is the Signal-to-Noise ratio at the receiver. Fig. 6 shows the capacity of the MIMO system considering different SNR, for both analyzed cases.

As observed in Fig. 6, the capacity estimation for the MIMO approximation is lower than the full MIMO 3D-RL simulated channel in both cases. This is related to the planar wavefront assumption and the different multipath contributions approximated along all antenna elements using the aforementioned postulation. This inference is more precise at higher frequencies and compact MIMO systems, given that they have a more reduced total effective antenna area than lower frequencies systems and spatial coherence is higher. Even so, dramatic phase changes occur in proportionally lower distances, and miss calculations in capacity estimations are bound to take place. The difference in capacity reaches a maximum of 9.4 bits and 11 bits per channel use in a 30 dB SNR channel conditions, for the 4-ULA and 16-UPA antennas, respectively. It must be remarked that the analysis of mmWave channel links considering line-of-sight conditions, as the presented in this letter, tends to have a lower number of time clusters and spatial lobes comparing than in microwave channel links, thus, limiting achievable multiplexing gains [12].

## V. CONCLUSION

This letter describes the addition of a geometric approximation method for MIMO antenna type free communication channel response in an in-house 3D-RL algorithm. The use of this method achieves a 93.4% reduction in simulation computational time, increasing by several orders the temporal efficiency of a MIMO channel simulation. The algorithm is performed in a postprocessing stage to the 3D-RL algorithm, and natively coupled to the software for nonstationarity simulations. The comparative results show that the approximation reflects the main characteristics of the real channel in the synthesized elements. In addition, the novel approximation method integrates all kind of antennas layout into a single calculation form. Due to its self-represented coordinate system, the orientation of the array is embedded and can easily be set up to follow temporal changes throughout the simulation. Also, given the signed nature of the point-plane distance, there is no need to assign an extreme point as the virtual point simulation. Thus, any element in the 3D array can be chosen, or no element at all, given a more logical use of a central array point, to exploit spatial coherence.

## REFERENCES

[1] J. Weng, X. Tu, Z. Lai, S. Salous, and J. Zhang, "Indoor massive MIMO channel modelling using ray-launching simulation," *Int. J. Antennas Propag.*, vol. 2014, 2014, Art. no. 279380.

[2] K. H. Ng, E. K. Tameh, and A. R. Nix, "Modelling and performance prediction for multiple antenna systems using enhanced ray tracing," in *Proc. IEEE Wireless Commun. Netw. Conf.*, 2005, pp. 933–937.

[3] O. Stabler and R. Hoppe, "MIMO channel capacity computed with 3D ray tracing model," in *Proc. 3rd Eur. Conf. Antennas Propag.*, 2009, pp. 2271–2275.

[4] S. Li, P. J. Smith, P. A. Dmochowski, H. Tataria, M. Matthaiou, and J. Yin, "Massive MIMO asymptotics for ray-based propagation channels," *IEEE Trans. Wireless Commun.*, vol. 19, no. 6, pp. 3977–3991, Jun. 2020.

[5] X. Cheng and Y. He, "Channel modeling and analysis of ULA massive MIMO systems," in *Proc. 20th Int. Conf. Adv. Commun. Technol.*, 2018, pp. 411–416.

[6] H. Jiang et al., "Approximation algorithm based channel estimation for massive MIMO antenna array systems," *IEEE Access*, vol. 7, pp. 149364–149372, 2019.

[7] C. Han and Y. Chen, "Propagation modeling for wireless communications in the terahertz band," *IEEE Commun. Mag.*, vol. 56, no. 6, pp. 96–101, Jun. 2018.

[8] I. Trindade, F. Muller, and A. Klautau, "Accuracy analysis of the geometrical approximation of MIMO channels using ray-tracing," in *Proc. IEEE Latin Amer. Conf. Commun.*, Nov. 2020, pp. 1–5.

[9] L. Azpilicueta, F. Falcone, and R. Janaswamy, "A hybrid ray launching-diffusion equation approach for propagation prediction in complex indoor environments," *IEEE Antennas Wireless Propag. Lett.*, vol. 16, pp. 214–217, 2017.

[10] L. Azpilicueta, M. Rawat, K. Rawat, F. Ghannouchi, and F. Falcone, "A ray launching-neural network approach for radio wave propagation analysis in complex indoor environments," *IEEE Trans. Antennas Propag.*, vol. 62, no. 5, pp. 2777–2786, May 2014.

[11] D. Tse and P. Viswanath, *Fundamentals of Wireless Communication*. Cambridge, U.K.: Cambridge Univ. Press, 2005.

[12] S. A. Busari, K. M. S. Huq, S. Mumtaz, L. Dai, and J. Rodriguez, "Millimeter-wave massive MIMO communication for future wireless systems: A survey," *IEEE Commun. Surveys Tuts.*, vol. 20, no. 2, pp. 836–869, Apr.-Jun. 2018.